ORIGINAL ARTICLE

Partial volume correction incorporating Rb-82 positron range for quantitative myocardial perfusion PET based on systolic-diastolic activity ratios and phantom measurements

Nils P. Johnson, MD,[a] Stefano Sdringola, MD,[b] and K. Lance Gould, MD[b]

Background. **Quantitative myocardial PET perfusion imaging requires partial volume corrections.**

Methods. **Patients underwent ECG-gated, rest-dipyridamole, myocardial perfusion PET using Rb-82 decay corrected in Bq/cc for diastolic, systolic, and combined whole cycle ungated images. Diastolic partial volume correction relative to systole was determined from the systolic/ diastolic activity ratio, systolic partial volume correction from phantom dimensions comparable to systolic LV wall thicknesses and whole heart cycle partial volume correction for ungated images from fractional systolic-diastolic duration for systolic and diastolic partial volume corrections.**

Results. **For 264 PET perfusion images from 159 patients (105 rest-stress image pairs, 54 individual rest or stress images), average resting diastolic partial volume correction relative to systole was 1.14 ± 0.04, independent of heart rate and within ±1.8% of stress images (1.16 ± 0.04). Diastolic partial volume corrections combined with those for phantom dimensions comparable to systolic LV wall thickness gave an average whole heart cycle partial volume correction for ungated images of 1.23 for Rb-82 compared to 1.14 if positron range were negligible as for F-18.**

Conclusion. **Quantitative myocardial PET perfusion imaging requires partial volume correction, herein demonstrated clinically from systolic/diastolic absolute activity ratios combined with phantom data accounting for Rb-82 positron range. (J Nucl Cardiol 2011;18:247–58.)**

Key Words: PET-CT imaging • partial volume correction • myocardial perfusion

doi:10.1007/s12350-010-9327-y

INTRODUCTION

Measuring absolute myocardial perfusion in cc/min/g at rest and stress, with absolute coronary flow reserve, is important for quantifying severity of coronary artery disease to guide management.[1-9] Percent narrowing of focal stenosis is inadequate for assessing severity or functional significance due to superposition of diffuse coronary atherosclerosis, multiple stenoses, heterogeneous remodeling, and heterogeneous endothelial dysfunction.[1-14] These anatomic and physiologic complexities cause a weak correlation between percent stenosis, coronary flow reserve, fractional flow reserve, or absolute maximal perfusion in cc/min/g in clinical studies.[13,14]

Cardiac positron emission tomography (PET) offers noninvasive measurement of absolute myocardial perfusion in cc/min/g.[1-9,15] However, quantitative cardiac

PET requires correction for partial volume loss associated with borderline reconstructed resolution for left ventricular (LV) wall thickness of 1.0 to 1.5 cm or less. Consequently, systolic images of gated cardiac PET have visually greater myocardial intensity and quantitative myocardial count density than diastolic images.[16] Quantitative myocardial activity in Bq/cc or µCi/cc of systolic images by PET is correspondingly higher than diastolic images. Lower diastolic count recovery compared to systole can produce artifactual inhomogeneity on ungated studies in normal subjects.[17]

Differences between systolic and diastolic quantitative recovery of absolute myocardial activity using ECG-gated cardiac PET arise from greater partial volume loss caused by thinner diastolic LV wall thickness compared to systolic LV wall thickness. Therefore, we determined: (i) the ratio of diastolic to systolic myocardial activity on ECG-gated PET images as the partial volume loss on diastolic images relative to systolic images and corresponding partial volume correction on diastolic images relative to systolic images. (ii) The different proportional contribution of systolic-diastolic activity to whole heart cycle, ungated perfusion images for different heart rates that may change the partial volume correction for whole heart cycle ungated images. (iii) The partial volume loss and partial volume correction for Rb-82 compared to F-18 for the same phantom target sizes since positron range of Rb-82 is substantially larger than the minimal positron range of F-18. (iv) The partial volume loss and partial volume correction for Rb-82 for phantom target widths of 0.5 to 3.0 cm that include the range of systolic and diastolic left ventricular wall thicknesses.

MATERIALS AND METHODS

Study Patients

We studied patients undergoing diagnostic myocardial perfusion rest-dipyridamole PET for potential coronary artery disease (CAD) or follow-up imaging at the Weatherhead PET Center for Preventing and Reversing Atherosclerosis of University of Texas Medical School-Houston and Memorial Hermann Hospital. All subjects signed a clinical informed consent approved by the Committee for the Protection of Human Subjects of University of Texas Health Science Center and Memorial Hermann Hospital.

PET Acquisition Protocol

Patients were instructed to fast for 4 hours and abstain from caffeine, theophylline, and cigarettes for 24 hours. Cardiac PET was performed using a Discovery ST 16-slice PET-computed tomography (CT) multislice bismuth germanate tomograph (GE Healthcare) in two-dimensional mode with extended septa and settings for theoretical in-plane resolution of 5.9 mm full width at half maximum (FWHM) as defined by NEMA standards in GE Discovery 16 slice PET-CT operations manual. However, reconstruction parameters and filters used clinically for cardiac PET-CT substantially reduce this resolution such that direct verification of quantifying activity for a range of target dimensions is essential.

Patients were positioned in the scanner using laser guides aligned to base of the throat and confirmed by CT scout scan. External body markers were used to ensure correct positioning throughout data acquisition. Emission images were obtained over 6 minutes after intravenous injection of 1,295-1,850 MBq (35-50 mCi) of generator-produced Rb-82 and contained 24-60 million total counts, of which 12-30 million were true coincidence counts.

Immediately after completing resting Rb-82 scan, dipyridamole (0.142 mg/kg/min) was infused for 4 minutes. Four minutes after completion of dipyridamole infusion, the same dose of Rb-82 was given intravenously. Emission image acquisition was started at 70 seconds (or 80 seconds for patients with heart failure or heart rates below 55 beats per minute, bpm) after beginning Rb-82 infusion. For dipyridamole-induced angina, aminophylline (125 mg) was given intravenously.

True coincidence counts were divided into eight equal-sized temporal R-R bins by ECG gating. CT scans for attenuation correction were acquired before rest emission imaging and after stress emission imaging. Protocols for CT acquisition, custom software to align PET emission and CT attenuation, data acquisition, processing and quantification of cardiac PET are as previously reported.[18-25]

Image Reconstruction

Images were reconstructed using filtered back projection with a Butterworth filter having a cutoff of 0.55, roll-off of 10, and pixel size of 3.27 × 3.27 mm. After attenuation correction, reconstructed PET emission images in DICOM format with quantitative header data were exported to an Ultra 60 workstation (Sun Microsystems) of an mPower-HZL PET scanner (Positron Corporation) running CARDIAC version 4.66 software for reorientation into long- and short-axis tomographic and topographic three-dimensional displays using previously described quantitative software.[19-25]

Three-dimensional restructuring algorithm generates true short- and long-axis views from reconstructed PET transaxial cardiac images, perpendicular and parallel to long axis of left ventricle. From tomographic data, circumferential profiles of maximum radial activity for each short axis slice are used to reconstruct three-dimensional topographic views of entire LV and lateral, inferior, septal, and anterior quadrant views of three-dimensional topographic displays corresponding to coronary artery distributions as previously described.[19-25]

Quantitative PET Image Analysis

Absolute activity recovered by the GE scanner was computed by converting raw counts to activity in Bq/cc and

µCi/cc using a linear calibrated GE-to-Positron conversion program validated by comparing PET measured F-18 activity in 8 and 20 cm cylindrical phantoms decay corrected from well counter quantification, imaged and quantified in the GE PET-CT compared to exported data quantified on the Positron workstation. Of 8 ECG-gated R-R bins, bins 3 and/or 4 after start of QRS complex were taken as systole and remaining bins 1, 2, 4, or 5 through 8 were taken as diastole based on those bin images best bracketing systole visually for each case. In some instances, bin 3 or 4 alone bracketed systole completely. Images representing diastole, systole, and both diastole plus systole added together as whole heart cycle images were decay corrected and converted to absolute activity in Bq/cc and µCi/cc in 1 second. A ratio image of systolic to diastolic activity was also created.

Ejection fraction was computed by semi-automated, endocardial-epicardial border tracking algorithm of Emory Toolbox program.[26] LV diastolic dimension was computed using a mid-cavity slice from circumferential profiles used to reconstruct three-dimensional topographic views of the ventricle during diastolic bins.

Relative Duration of Systole and Diastole for Heart Rate

Body-mass index in units of kg/m^2 was computed as weight divided by square of height measured at PET imaging. Heart rate was determined from 12-lead stress test ECG monitor and recorded log at beginning of image acquisition and was constant throughout short image acquisition times for Rb-82. An additional 3-lead monitor was used for ECG gating of PET images.

The reported relationship between heart rate and proportion of R-R interval spent in systole[27] used the following formulae:

Systolic fraction of R-R interval $= RR_{sys} =$

$$0.01 * \exp(4.14 - 40.74/\text{heart rate}), \qquad (1)$$

Diastolic fraction of R-R interval $= RR_{dia}$

$$= 1 - RR_{sys}, \qquad (2)$$

where heart rate is in beats per minute (bpm). Alternatively, the more simplistic assumption that 1/3 of the R-R interval represents systole ($RR_{sys} = 1/3$) and 2/3 of R-R interval represents diastole ($RR_{dia} = 2/3$), independent of heart rate, was also examined.

Partial Volume Correction and Relative Systolic Diastolic Duration

If cardiac PET images had no partial volume loss (partial volume correction = 1.0), diastolic and systolic myocardial absolute activity in µCi/cc would be identical. Total partial volume correction for combined systolic and diastolic image (ungated whole cycle images) depends on partial volume correction (or partial volume loss) for diastole (D_{pvc}), on partial volume correction for systole (S_{pvc}), and on the relative

proportion or fraction of R-R interval spent in systole (RR_{sys}) and diastole (RR_{dia}). Total partial volume correction (T_{pvc}) is therefore given by:

$$T_{pvc} = RR_{sys} \times S_{pvc} + RR_{dia} \times D_{pvc} \qquad (3)$$

As a first step, the diastolic partial volume correction relative to systole is determined by arbitrarily setting the systolic partial volume correction $S_{pvc} \approx 1.0$, to be corrected as appropriate in a second step. Thus, diastolic partial volume correction relative to systole is then given by systolic/diastolic ratio of absolute activity ($AA_{s/d}$). Total partial volume correction equation relative to a systolic partial volume correction of 1.0 then becomes:

$$T_{pvc} = RR_{sys} + (1 - RR_{sys}) \times AA_{s/d} \qquad (4)$$

This first step of the analysis is necessary to quantify on clinical gated PET perfusion images the systolic-diastolic differences and the diastolic partial volume correction relative to systole.

The next steps of the analysis require (i) measuring partial volume loss and partial volume correction from activity profiles of different phantom target sizes of known widths and activity concentrations for both Rb-82 and F-18 to define separate and combined effects of positron range and spreading function of reconstructed images on partial volume loss over target sizes comparable to left ventricular wall thicknesses, here 0.5 to 3 cm widths (ii) from these profiles, determine partial volume loss for *systolic* wall thickness due to positron range and spreading function of reconstructed images (iii) combine or integrate diastolic partial volume correction based on ECG-gated PET images with systolic partial volume correction based on peak values of phantom activity profiles.

Theoretical Effects of Rb-82 Positron Range, Partial Volume Loss and Physical Target Dimensions

Positron range of Rb-82 averages 2 to 4 mm but ranges non-linearly up to 14 mm (Table 1).[28-31] Consequently, positrons emitted next to physical target boundaries may travel beyond and decay outside physical boundaries of the target such that activity concentration next to physical boundaries is less than in central regions that are larger than positron range with no positron activity lost to outside the physical boundaries.

Therefore, as a result of positron range, size of the radioactive target is changed as illustrated in Figure 1. For physical target widths of 1.0 cm approximating diastolic wall thickness and 1.5 cm approximating systolic wall thickness, Figure 1 shows a simulation of these target dimensions convolved with published range distribution of Rb-82 positrons[32,33] and then further convolved with a Gaussian spreading function for reconstructed PET images of 9 mm full width half maximum based on experimental data as described below for F-18 incorporating scanner intrinsic resolution reported as 5.9 mm[34] in addition to effects of smoothing filters.

In Figure 1, if rubidium activity is followed to 80% of its peak, it is smaller than physical boundaries of the target with lower peak activity due to positron range outside both sides of

Table 1. Positron ranges

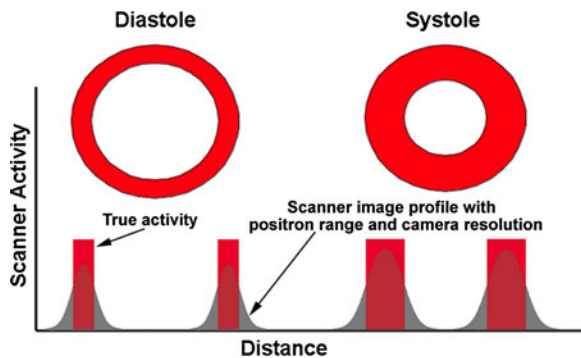| Radionuclide	Positron ranges reported (mm)
Rb-82 ave 3.85 mm	5.9, 4.29, 2.60, 2.6, max 14.1
F-18 ave 0.36 mm	0.64, 0.23, 0.2
N-13 ave 1.1 mm	1.4, 1.32, 0.57

From Refs.[28-31]

Figure 1. Simulation (*grey*) of 1.0 (*left*, diastole) and 1.5 cm (*right*, systole) ideal targets (*red*) convolved with published range distribution of Rb-82 positrons[33] and then further convolved with an empiric Gaussian spreading function of 9 mm FWHM for reconstructed PET images.

physical target boundaries. If rubidium activity is followed down to 20% of its peak, it is larger than physical boundaries of the target to the extent of positron range or longer tails outside both sides of physical target boundaries. Activity profile of Rb-82 will therefore be narrower than for F-18 at 80% of peak. The peak will be lower and partial volume loss for Rb-82 will be larger than for F-18 for targets of 1 to 2 cm wide characteristic of left ventricular wall thickness at or below the limits of scanner resolution for 100% recovery of peak target activity.

This theoretical simulation was then compared to measured activity recovery from phantoms of comparable dimensions filled with Rb-82 for determining the final composite partial volume correction accounting for both Rb-82 range and spreading function of reconstructed images.

Phantom Studies

A tree-like phantom (Mullani ''tree'' phantom) with angled branches of varying widths, machined 4 cm deep, illustrated in Figure 2[35] was scanned after being filled by F-18 and separately by Rb-82 with activity precisely measured by well counter, or a fresh rubidium infusion system, in known volume with precisely timed decay correction starting from well counter or infusion system measurement to imaging. On images of the tree phantom filled with Rb-82 or F-18, activity profiles were obtained using a round region of interest (ROI) of
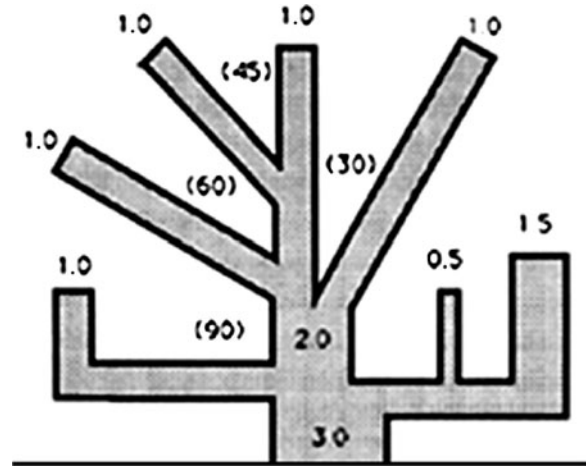

Figure 2. Schematic of the tree-like phantom (Mullani ''tree'' phantom[21] with angled branches of varying width filled with known uniform activity of Rb-82 and F-18 for comparison to PET measured activity for determining partial volume loss and corrections. *Numbers* indicate width of each tree branch in centimeters and *numbers* in *parenthesis* indicate the angle in degrees off the vertical.

0.85 mm radius where viewing software interpolates the 3.27 mm isotropic raw data. This ROI was stepped perpendicular to each ''tree'' branch across it in 0.85 mm steps for the 3.0, 2.0, 1.5, 1.0, and 0.5 cm wide branches of the tree phantom. Recovered activity in each ROI was determined by converting raw counts to activity in Bq/cc and μCi/cc using the GE commercial calibration confirmed by a linear calibrated conversion formula validated in prior 8.0 and 20.0 cm diameter cylindrical phantoms filled with known activity of F-18 by well counter.

For each small ROI on the tree phantom, the ratio of ROI recovered activity to true peak activity (ROI/true peak) was measured as the partial volume loss. Peak scanner measured activity per cc in the central 3.0 cm branch or trunk of the tree phantom was slightly *higher* than calculated activity concentration for both Rb-82 and for F-18 due to underestimation of decay correction from well counter measurement for F-18 or from generator infusion of Rb-82 into mixing beaker, to filling the tree phantom without bubbles, to positioning and to imaging. Consequently, peak scanner measured activity in the ROI of 0.85 mm radius located in the central 3.0 cm arm was used as true peak activity in Bq/cc or μCI/cc for determining the ratio of measured ROI activity to true peak activity for all other ROI measurements for all other locations across all the branches of the tree phantom (ROI/true peak).

Combined Diastolic Partial Volume Corrections and Phantom Data

Diastolic partial volume correction compared to systole on ECG-gated images may underestimate partial volume correction for the whole heart cycle images to the extent of any partial volume loss for systolic images. Systolic partial volume loss and partial volume correction was determined from peak

Table 2. Left ventricular systolic wall thickness

First author	Citation	Year	N	Tool	LV_{sys} (mm)
Eber	Circulation 39:455–64	1969	6	XR	17.1 ± 1.9
Frick	J Appl Physiol 29:452–5	1970	22	echo	13.7 ± 2.0
Feneley	Circulation 70:226–32	1984	18	echo	13.3 ± 1.5
Fisher	AJR 145:27–30 (6–9 pts)	1985	7	MRI	14.4 ± 2.1
Kaul	AJR 146:75–9	1986	9	echo	14.8 ± 1.9
Kaul	AJR 146:75–9	1986	16	MRI	16.0 ± 2.9
Semelka	Radiology 174:763–8	1990	11	MRI	16.4 ± 1.6
Freiberg	JNC 11:38–46	2004	12	MRI	17.0 ± 4.0
Freiberg	JNC 11:38–46	2004	12	PET	17.0 ± 2.0
Weighted average			113	All	15.1 ± 0.7
Weighted average ECHO			48	Echo	13.7 ± 1.1
Weighted average MRI			48	MRI	15.9 ± 0.7

values of activity profiles across different sized branches of the tree phantom within the published range of systolic wall thicknesses (Table 2). This systolic partial volume correction based on peak activity concentration of tree phantom activity profiles was then used in Eq. 3 above with the diastolic partial volume correction from ECG-gated PET images and relative systolic diastolic time intervals to calculate partial volume correction for quantitative myocardial uptake of the whole heart cycle ungated images.

Statistical Methods

All statistical tests were performed using STATA version 10.1 (StataCorp, College Station, Texas). Continuous variables are expressed as mean ± standard deviation and were compared using the *t* test. Paired data was compared using paired *t* test. All applicable tests were two-tailed, and a $P < .05$ was taken as cutoff for statistical significance.

RESULTS

Diastolic Partial Volume Loss Relative to Systolic Images on ECG-Gated Images

Figure 3A illustrates tomographic views of relative myocardial activity in diastole and systole scaled to maximum activity of the entire image data set. Systolic images have 18% more activity than diastolic images in this example when systolic and diastolic images are normalized or scaled to same maximum activity. Although myocardial activity is the same in diastole and systole, diastolic images appear to have less activity and more heterogeneity than systolic images due to greater partial volume loss caused by thinner LV wall during
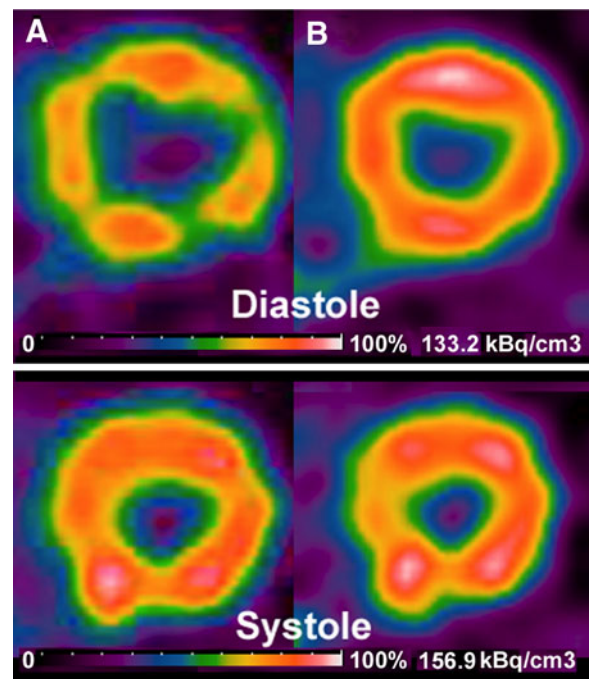

Figure 3. Diastolic and systolic PET images of Rb-82. **A** PET tomographic views of relative myocardial activity in diastole and systole scaled relative to maximum activity of entire data set (100%). Systolic images have 18% more activity than diastolic images in this example when systolic and diastolic images are normalized or scaled to the same maximum activity. **B** PET tomographic views of absolute myocardial activity in kBq/cc, where diastole and systole are normalized to their own maximum that is scaled to the separate maximum kBq/cm^3 of diastole (133.2) and systole (156.9). Since diastolic and systolic images are scaled to their own maximum, images look similar other than the smaller systolic LV cavity but the absolute quantitative scale defines quantitative differences.

diastole. Figure 3B shows this same data set converted to absolute activity in kBq/cc where diastole and systole are separately normalized to their own maximum that is scaled to the separate maximum kBq/cc of diastole and systole by Positron quantitative software. Since diastolic and systolic images are scaled to their own maximum, the images look similar other than smaller systolic LV cavity size but different absolute quantitative scale for diastole and systole defines quantitative differences.

A total of 159 patient studies produced 105 paired (rest and stress) images and 54 individual (rest or stress) images for a total of 264 PET acquisitions, all without atrial fibrillation and majority with normal ($\geq$55%) ejection fraction (220 of 264 acquisitions). Only 4 studies had ejection fraction (EF) <40%, and no study had EF <34%. Patients were selected from the entire spectrum of coronary artery disease, including asymptomatic patients for screening, stable or unstable angina, past myocardial infarction, second opinions, or patients appropriate for revascularization procedures.

Table 3 shows clinical and imaging parameters for all PET acquisitions. Activity recovery in systole is higher (1.90 μCi/cc) compared to diastole (1.57 μCi/cc), $P <$ .0001 for a difference of 0.32 $\pm$ 0.13 μCi/cc. Average partial volume correction factor is 1.14 for assumed 1/3 systolic and 2/3 diastolic fractions of RR interval regardless of heart rate. Alternatively, average partial volume correction adjusted for systolic-diastolic fractions at different heart rates for each image is also 1.14 with a slight statistical difference (difference = 0.004 $\pm$ 0.056, $P <$ .0001). Therefore, partial volume corrections with and without accounting for individual heart rates for each image are identical for clinical purposes.

Partial Volume Correction Over a Wide Range of Heart Rates

Table 4 computes theoretical partial volume correction relative to systole having no partial volume loss over a wide range of heart rates using the average systolic/diastolic activity ratio from Table 3. Partial volume correction remains similar regardless of heart rate even at extremes of 45 and 100 bpm that show 1.8% ([1.16-1.14]/1.16) or ([1.14-1.12]/1.14) over or under partial volume correction at an intermediate heart rate of 71. Therefore, it is not necessary to adjust systolic-diastolic partial volume correction for individual heart rate in each image for heart rates of 45 to 100 bpm seen with dipyridamole stress.

Rest Versus Stress Images

Table 5 shows clinical and imaging parameters for all 105 paired rest and stress acquisitions. While

Table 3. Observed parameters

	Mean $\pm$ SD
Heart rate (bpm)	71 $\pm$ 19
Diastolic whole heart absolute uptake (μCi/cc)	1.57 $\pm$ 0.50
Systolic whole heart absolute uptake (μCi/cc)	1.90 $\pm$ 0.59
Systolic/diastolic activity ratio (AA$_{s/d}$)	1.21 $\pm$ 0.06
Diastolic and systolic whole heart uptake (μCi/cc)	1.60 $\pm$ 0.52
Partial volume correction (systole = 1/3 diastole = 2/3)*	1.14 $\pm$ 0.04
Partial volume correction (based on heart rate)**	1.14 $\pm$ 0.04
Fraction of R-R spent in systole (RR$_{sys}$)***	0.34 $\pm$ 0.05
Diastolic LV diameter (cm)	5.2 $\pm$ 0.7
Ejection fraction (%)	64.4 $\pm$ 10.4
Weight (lbs)	189.1 $\pm$ 37.1
Body-mass index (kg/m^2)	27.9 $\pm$ 4.9

Note: N = 264 except for weight and body-mass index which are N = 159.
* Using Eq. 4 with RR$_{sys}$ = 1/3 and RR$_{dia}$ = 2/3.
** Using Eq. 4 with RR$_{sys}$ from Eq. 1 and RR$_{dia}$ from Eq. 2.
*** Using Eq. 1.
bpm, Beats per minute; *LV*, left ventricle; *SD*, standard deviation.

statistically different, partial volume corrections for rest (1.14 $\pm$ 0.03) and stress (1.16 $\pm$ 0.04) are clinically comparable, within 1.8% of each other relative to systole images with no partial volume loss.

Activity Profiles for Phantom Dimensions for F-18 and Rb-82

Figure 4 shows the tree phantom filed with Rb-82 (Panel A) and with F-18 (Panel B), in color and in black and white display with activity scales for each. Compared to F-18, the color Rb-82 image of the phantom has comparable visual peak intensity in the 3.0 and 2.0 cm branches but lower visual peak intensity in the smaller branches. Grey scale images show broadening of Rb-82 images compared to F-18 due to greater positron range of Rb-82. Solid narrow lines show paths of the round ROI of 0.85 mm radius stepped across each branch in 0.85 mm increments perpendicular to it. The small rectangular ROI is 1 cm tall in scanner space as a size reference corresponding to the 1 cm physical width of the 1.0 cm wide phantom branch.

Figure 5 shows activity profiles across the 3.0, 2.0, 1.5, and 1.0 cm dimensions of the tree phantom. The

Table 4. Theoretical partial volume corrections by heart rate

Heart rate (bpm)	Systolic fraction*	Diastolic fraction**	Correction equation***	Partial volume correction
45	0.25	0.75	$0.25 + 0.75 \times 1.21$	1.16
59	0.31	0.69	$0.31 + 0.69 \times 1.21$	1.15
71	0.35	0.65	$0.35 + 0.65 \times 1.21$	1.14
87	0.39	0.61	$0.39 + 0.61 \times 1.21$	1.13
100	0.42	0.58	$0.42 + 0.58 \times 1.21$	1.12

* Using Eq. 1.
** Using Eq. 2.
*** Using Eq. 4 and $AA_{s/d}$ = 1.21 from Table 1.

Table 5. Paired rest and stress observations

	Rest	Stress	*P*
Heart rate (bpm)	59 ± 12	87 ± 17	<.0001
Diastolic whole heart absolute uptake (μCi/cc)	1.45 ± 0.48	1.56 ± 0.47	<.0001
Systolic whole heart absolute uptake (μCi/cc)	1.75 ± 0.56	1.94 ± 0.57	<.0001
Ungated whole heart absolute uptake (μCi/cc)	3.15 ± 0.96	3.93 ± 1.13	<.0001
Systolic/diastolic activity ratio ($AA_{s/d}$)	1.21 ± 0.04	1.24 ± 0.05	<.0001
Partial volume correction (systole = 1/3 diastole = 2/3)*	1.14 ± 0.03	1.16 ± 0.04	<.0001
Ejection fraction (%)	62.7 ± 8.6	68.5 ± 10.2	<.0001
Diastolic LV diameter (cm)	5.3 ± 0.6	5.1 ± 0.7	<.0001

N = 105 for all rows.
* Using Eq. 4 with RR_{sys} = 1/3 and RR_{dia} = 2/3.
bpm, Beats per minute; *LV,* left ventricle.

maximum for the Rb-82 scale is 184.630 Bq/cc (4.99 μCi/cc) and for the F-18 scale 498,202 Bq/cc (13.46 μCi/cc) that is the true activity, decreases from which in each ROI are due to partial volume loss expressed as the ratio of ROI/true peak. For the 3 cm wide dimension of the tree phantom, peak activity of both radionuclides is the same with the ratio of PET measured to true peak (ROI/true peak) of 1.0. However, the Rb-82 profile has narrower peak activity within the 3.0 cm physical dimension and is broader with more tails of activity outside the phantom dimensions due to the positron range of Rb-82, as predicted by the simulation in Figure 1.

For the 2.0 cm wide branch, peak activity of Rb-82 is 4% lower than true peak activity compared to 0.4% for F-18 (Table 6) due to the radioactive size of the 2.0 cm branch at peak being smaller for Rb-82 than for F-18 due to positron range, with a corresponding 4% partial volume loss for Rb-82 versus only 0.4% for F-18. For the 1.5 cm wide branch, the true peak Rb-82 activity is 12.3% lower than the true peak activity and the peak F-18 peak activity is 5.3% lower than true peak activity (Table 6). Consequently, Rb-82 has greater partial volume loss associated with the smaller peak radioactive target width due to its large positron range that is proportionately greater for 1.5 cm than for larger dimensions.

For the 1.0 cm wide branch, peak radioactive Rb-82 target is proportionately still smaller than physical target dimensions due to positron range and associated partial volume loss is 30.9% for Rb-82 compared to 20.4% for F-18. Finally, for the 0.5 cm branch, partial volume loss for Rb-82 is 51.2% compared to 42.4% for F-18 (Table 6). Areas under the profiles for Rb-82 and F-18 are comparable with the average ratio of area under the F-18 profile to area under the Rb-82 profile being 0.97 ± 0.03 for the 0.5 to 3.0 cm phantom dimensions.

Positron range of F-18 is small, approximately 0.36 mm (Table 1). Since positron range for F-18 is small, deconvolution of F-18 profiles to fit each phantom dimension gives the composite spreading function for reconstructed images that includes intrinsic scanner resolution and effects of smoothing filters, here assumed to be a Gaussian with a full width half maximum value of 9 mm based on the experimental data. Theoretically predicted partial volume corrections for Rb-82 and F-18 were determined by convolving the phantom dimension with the published range distribution for Rb-82 that was
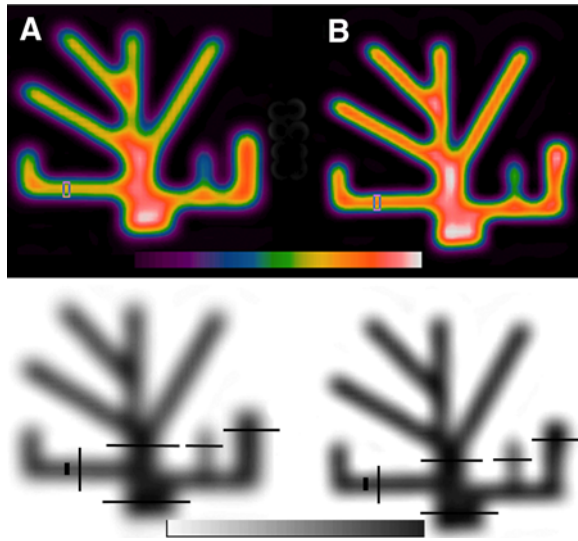
Figure 4. PET images of tree phantom filled with Rb-82 (panel **A**) and separately with F-18 (panel **B**), with *color scale* above and the same images in *black* on *white* below. Maximum activity of *bar* scale for Rb-82 is 184.630 Bq/cc (4.99 µCi/cc) and for F18 is 498,202 Bq/cc (13.46 µCi/cc) for both *color* and *black* on *white* displays. The small rectangular ROI is 1 cm tall in scanner space as size reference corresponding to 1 cm physical width of that phantom branch. The *narrower lines* indicate the path of the ROI of 0.85 mm radius stepped across the phantom branches in 0.85 mm increments for measuring profiles of quantitative activity.

further convolved with the composite spreading function for reconstructed images, as illustrated in Figure 1. These predicted partial volume corrections were then compared to those determined from direct peak activity measurements from the phantoms for each radionuclide, Figure 6.

Figure 6 graphs measured partial volume corrections versus target size for Rb-82 and F-18 illustrating that partial volume correction for Rb-82 averages 7.2% (Table 6) more than F-18 for the 0.5 to 1.5 cm targets due to Rb-82 positron range. Grid lines provide estimates of partial volume corrections for intermediate sizes among the primary dimensions at which measurements were made. Dashed lines indicate theoretically predicted relation from the simulation illustrated in Figure 1.

Since partial volume correction for F-18 for the 1.5 to 3.0 cm phantom dimension is essentially 1.0 (Table 6), the F-18 data for phantom dimensions serves as an approximate reference for partial volume corrections without the positron range of Rb-82. Therefore, comparison of Rb-82 with F-18 provides the approximate effects of Rb-82 positron range for the same scanner with same settings, same spreading function of reconstructed images and same physical target dimensions.

Combined Diastolic Systolic and Phantom Partial Volume Corrections for Clinical PET

From Table 6, partial volume loss for a systolic dimension of 1.5 cm for Rb-82 is 12.3%. From Table 3, average diastole partial volume loss compared to systole is 21%. Therefore, total diastolic partial volume loss with a 1.5 cm systolic LV wall thickness would be an additional 21% more than the 12.3% partial volume loss of the systolic wall thickness, for a total diastolic partial volume loss of 33.3%. In comparison, partial volume loss for Rb-82 for the 1.0 cm dimension of the phantom that approximates diastolic wall thickness is 31%.

Partial volume loss for the whole heart cycle for diastolic partial volume loss of 33.3% and systolic partial volume loss of 12.3% for a 1.5 cm systolic LV wall thickness can then determined for the proportional duration of systole and diastole from Eq. 3 above: $T_{pvc} = RR_{sys} \times S_{pvc} + RR_{dia} \times D_{pvc}$.

From Table 3, for a systolic duration of 0.34 and diastolic duration of 0.66, the whole heart cycle partial volume correction for ungated images is $T_{pvc} = (0.34)(1.123) + (0.66)(1.333) = 0.382 + 0.88 = 1.26$. Similarly, whole heart cycle partial volume corrections for can be made for different systolic wall thicknesses including thin-walled dilated hearts if systolic wall thickness is measured.

This systolic diastolic PET method for determining *diastolic* partial volume correction relative to systole and the phantom-based *systolic* partial volume corrections for systolic dimensions require that quantitative myocardial radionuclide uptake be determined as the peak value along a radius outward from the center of the left ventricle on short axis tomographic slices, as done in our software described above, corresponding to peak activities of the phantom profiles upon which partial volume corrections are based.

DISCUSSION

Our results support several conclusions. First, positron range of Rb-82 is large enough to alter radioactive target dimensions at peak activity and partial volume corrections for Rb-82 are somewhat greater than for F-18 that has a small positron range. Second, partial volume corrections with and without accounting for individual heart rates for each image are identical for clinical purposes for the range of heart rates seen with dipyridamole stress. Third, partial volume corrections for rest and stress PET perfusion images are clinically comparable. Fourth, this method combining diastolic-systolic activity differences and phantom data is applicable to any calibrated scanner and for a range of measured or assumed systolic wall thicknesses to define
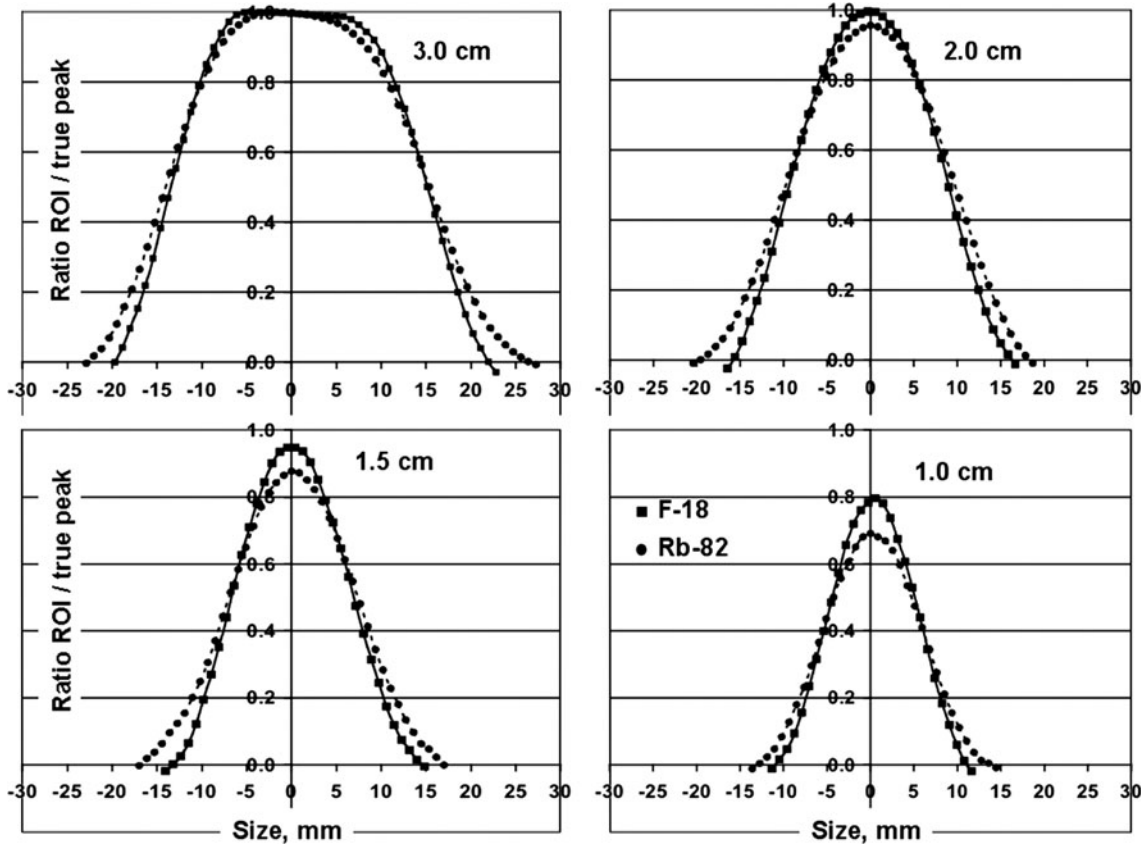
Figure 5. Activity profiles across different sized branches of the tree phantom for Rb-82 and F-18 expressed as the ratio of peak PET measured activity in the small ROI to true peak activity (ROI/ true peak) for each phantom dimension.

Table 6. Partial volume loss as ratio of pet/true by phantom dimension using small ROIs

Size (cm)	ROI/ true peak F-18	ROI/ true peak Rb-82	Fractional loss F-18	Fractional loss Rb-82	Partial vol correction F-18	Partial vol correction Rb-82	pv correction % Rb > F
3.0	1.0	1.0	0	0	1.0	1.0	0
2.0	0.996	0.956	0.004	0.04	1.004	1.04	3.6
1.5	0.947	0.877	0.053	0.123	1.053	1.123	6.6
1.0	0.796	0.691	0.204	0.309	1.204	1.309	8.7
0.5	0.576	0.488	0.424	0.512	1.424	1.512	6.2

Actual or true activity of Rb-82 in phantom = 184.630 Bq/cc (4.99 μCi/cc).
Actual or true activity of F18 in phantom = 498,202 Bq/cc (13.46 μCi/cc).
PET Bq/cc and μCi/cc = peak activity measured in ROI with radius of 0.85 mm stepped across each arm in 0.85 mm increments.

partial volume correction for whole heart cycle ungated images. Fifth, using MRI, CT, or ECHO to obtain physical dimensions as the basis for partial volume corrections does not account for positron range of Rb-82 that substantially reduces peak radioactive target size for objects 1.5 cm or less that makes partial volume loss

greater than expected based on physical dimension only. Our systolic-diastolic method accounts for positron range since both systole and diastole are equally affected by positron range.

These findings enable robust recovery of absolute myocardial activity necessary for quantitative perfusion
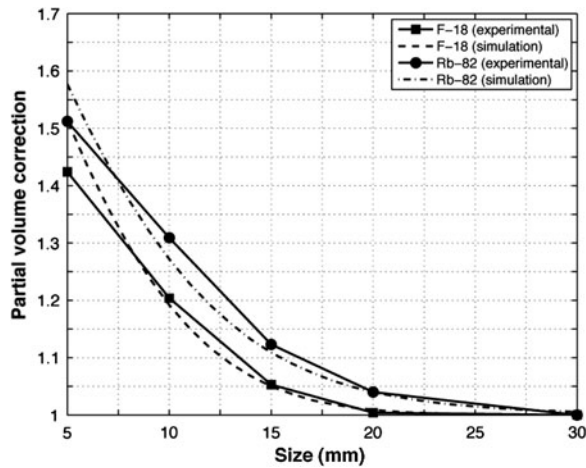
Figure 6. Partial volume corrections based on peak PET measured activity across each phantom dimension as a ratio to true peak activity for Rb-82 and F-18. The dashed lines indicate the theoretical curves derived from the simulation illustrated in Figure 1.

but with limitations and qualification outlined below. This method combining diastolic-systolic differences and phantom data may in principle be applied to an individual with specific individual regional systolic left ventricular wall size, thickening and heart rate at rest and stress for determining a specific individual whole heart cycle partial volume correction for quantifying myocardial radionuclide uptake on ungated images. However, for routine clinical application in our lab, individually determined partial volume corrections are comparable to average values determined for the 264 PET studies reported here with an acceptable narrow standard deviation. Therefore, we use this average value as a single fixed partial volume correction for all patients except that dilated, thin walled, poorly contracting hearts are undergoing further study for individualized application of our method. While not tested, our method should be applicable for reconstructed images by ordered subset expectation maximization (OSEM).

Comparison to Existing Literature

Systolic-diastolic activity differences have been used to estimate systolic wall thickening by gated PET.[16] However, if scanner resolution and quantitative recovery were optimal, systolic, and diastolic activity would be identical with no relation to systolic wall thickening. Therefore, empirical correlation of systolic-diastolic activity with wall thickening[16] reflects a characteristic of the scanner rather than a true physiological measurement. To the extent that systolic-diastolic activity parallels wall thickening, it also reflects

systolic-diastolic partial volume differences and partial volume corrections not addressed in prior papers.

Several alternative methods have been used to account for partial volume effects in cardiac PET imaging. Some have utilized anatomic information from other imaging modalities, such as echocardiography, magnetic resonance imaging, or CT to develop geometric models for partial volume correction incorporated into quantitative flow models. However, these approaches do not account for the positron range of Rb-82 that reduce peak activity target size sufficiently to alter partial volume corrections for target dimensions of 1.5 cm or smaller. In principle, these anatomic imaging modalities could be used with data of Table 6 or Figure 6 or comparable corrections for positron range to obtain correct partial volume corrections.

A popular model by Hutchins for PET partial volume correction incorporates an additional variable into the compartmental flow models.[36] While the Hutchins model offers the advantage of not assuming partial volume corrections beforehand, it simultaneously offers the disadvantage of an additional parameter that must be fit and could therefore destabilize the model. The flow model we use clinically offers greater stability at the price of less flexibility by demanding that the aortic and myocardial partial volume corrections be entered explicitly.[15]

Limitations of the Study

A sub-analysis of 12 patients with EF of 43% or lower, ranging 34 to 43, average 39.8 ± 1.8, had systolic/diastolic activity ratio of 1.17 ± 0.05 that is somewhat lower than the 1.21 ± 0.06 (Table 3) for all patients, as expected for less LV wall thickening. Diastolic-systolic partial volume correction for diastolic images determined by PET imaging could be added to systolic partial volume correction determined by measured systolic wall thickness by ECHO, MRI, or CT with its corresponding partial volume correction from Figure 6 that includes effects of rubidium positron range and comparable spreading function of reconstructed images.

However, we have not tested this approach for thin-walled regions of the left ventricle, for reduced systolic wall thickening, or with anatomic measurements of left ventricular wall thickness by other imaging modalities. PET scanners with different reconstruction filters, or different resolutions will require calibration by phantoms with dimensions comparable to the tree phantom used in this study.

Other high energy positron emitters, such as oxygen-15 with longer range than F-18 may also require larger partial volume corrections than expected based on physical target dimensions alone. Finally, greater

positron range in lung air space next to myocardium has an unknown effect not addressed here.

CONCLUSIONS

This study demonstrates that positron range of Rb-82 is accounted for in a robust method for partial volume corrections in quantitative cardiac PET based on systolic/diastolic ratios of absolute activity of ECG-gated perfusion images for *diastolic* partial volume correction combined with *systolic* partial volume correction from phantom activity profiles for dimensions comparable to systolic LV wall thickness. Average resting diastolic partial volume correction relative to systole was 1.14 ± 0.04, independent of heart rate and within ±1.8% of stress images (1.16 ± 0.04). *Diastolic* partial volume correction based on the systolic/diastolic activity ratio combined with *systolic* partial volume correction from phantom data for dimensions comparable to systolic LV wall thickness gave an average whole heart cycle partial volume correction for ungated images of 1.23 for Rb-82 compared to 1.14 if positron range were negligible as for F-18.

Open Access

References

1. Gould KL. Does coronary flow trump coronary anatomy? JACC Cardiovasc Imaging 2009;2:1009-23.
2. Di Carli MF, Dorbala S, Meserve J, El Fakhri G, Sitek A, Moore SC. Clinical myocardial perfusion PET/CT. J Nucl Med 2007;48:783-93.
3. Schelbert HR. Coronary circulatory function abnormalities in insulin resistance insights from positron emission tomography. J Am Coll Cardiol 2009;53:S3-8.
4. Schindler TH, Zhang XL, Vincenti G, Mhiri L, Nkoulou R, Just H, et al. Diagnostic value of PET-measured heterogeneity in myocardial blood flows during cold pressor testing for the identification of coronary vasomotor dysfunction. J Nucl Cardiol 2007;14:688-97.
5. Dorbala S, Hassan A, Heinonen T, Schelbert HR, Di Carli MF. Coronary vasodilator reserve and Framingham risk scores in subjects at risk for coronary artery disease. J Nucl Cardiol 2006;13:761-7.
6. Schindler TH, Nitzsche EU, Schelbert HR, Olschewski M, Sayre J, Mix M, Brink I, et al. Positron emission tomography-measured abnormal responses of myocardial blood flow to sympathetic stimulation are associated with the risk of developing cardiovascular events. J Am Coll Cardiol 2005;45:1505-12.
7. Hachamovitch R, Di Carli MF. Nuclear cardiology will remain the ''gatekeeper'' over CT angiography. J Nucl Cardiol 2007;14:634-44.
8. Ziadi MC, Beanlands RS. The clinical utility of assessing myocardial blood flow using positron emission tomography. J Nucl Cardiol 2010;17:571-81.
9. Bax JJ, Beanlands RS, Klocke FJ, Knuuti J, Lammertsma AA, Schaefers MA, et al. Diagnostic and clinical perspectives of fusion imaging in cardiology: Is the total greater than the sum of its parts? Heart 2007;93:16-22.
10. Topol EJ, Nissen SE. Our preoccupation with coronary luminology. The dissociation between clinical and angiographic findings in ischemic heart disease. Circulation 1995;92:2333-42.
11. De Bruyne B, Hersbach F, Pijls NH, Bartunek J, Bech JW, Heyndrickx GR, et al. Abnormal epicardial coronary resistance in patients with diffuse atherosclerosis but ''Normal'' coronary angiography. Circulation 2001;104:2401-6.
12. De Bruyne B, Pills NH, Heyndrickx GR, Hodeige D, Kirkeeide R, Gould KL. Pressure-derived fractional flow reserve to assess serial epicardial stenoses: Theoretical basis and animal validation. Circulation 2000;101:1840-7.
13. White CW, Wright CB, Doty DB, Hiratza LF, Eastham CL, Harrison DG, et al. Does visual interpretation of the coronary arteriogram predict the physiologic importance of a coronary stenosis? N Engl J Med 1984;310:819-24.
14. Meijboom WB, Van Maugham CA, van Pelt N, Weustink A, Pugliese F, Mollet NR, et al. Comprehensive assessment of coronary artery stenoses: Computed tomography coronary angiography versus conventional coronary angiography and correlation with fractional flow reserve in patients with stable angina. J Am Coll Cardiol 2008;52:636-43.
15. Yoshida K, Mullani N, Gould KL. Coronary flow and flow reserve by PET simplified for clinical applications using rubidium-82 or nitrogen-13-ammonia. J Nucl Med 1996;37:1701-12.
16. Yamashita K, Tamaki N, Yonekura Y, Ohtani H, Saji H, Mukai T, et al. Quantitative analysis of regional wall motion by gated myocardial positron emission tomography: Validation and comparison with left ventriculography. J Nucl Med 1989;30:1775-86.
17. Bartlett ML, Bacharach SL, Voipio-Pulkki LM, Dilsizian V. Artifactual inhomogeneities in myocardial PET and SPECT scans in normal subjects. J Nucl Med 1995;36:188-95.
18. Wollenweber SD, Gould KL. Investigation of cold contrast recovery as a function of acquisition and reconstruction parameters for 2D cardiac PET. IEEE Nucl Sci Symp Conf Rec 2005;5:2552-6.
19. Gould KL, Ornish D, Scherwitz L, Brown S, Edens RP, Hess MJ, et al. Changes in myocardial perfusion abnormalities by positron emission tomography after long-term, intense risk factor modification. JAMA 1995;274:894-901.
20. Gould KL, Martucci JP, Goldberg DI, Hess MJ, Edens RP, Latifi R, et al. Short-term cholesterol lowering decreases size and severity of perfusion abnormalities by positron emission tomography after dipyridamole in patients with coronary artery disease. A potential noninvasive marker of healing coronary endothelium. Circulation 1994;89:1530-8.
21. Sdringola S, Nakagawa K, Nakagawa Y, Yusuf SW, Boccalandro F, Mullani N, et al. Combined intense lifestyle and pharmacologic lipid treatment further reduce coronary events and myocardial perfusion abnormalities compared with usual-care cholesterol-lowering drugs in coronary artery disease. J Am Coll Cardiol 2003;41:263-72.
22. Gould KL. Assessing progression or regression of CAD: The role of perfusion imaging. J Nucl Cardiol 2005;12:625-38.

23. Sdringola S, Loghin C, Boccalandro F, Gould KL. Mechanisms of progression and regression of coronary artery disease by PET related to treatment intensity and clinical events at long-term follow-up. J Nucl Med 2006;47:59-67.

24. Gould KL, Pan T, Login C, Johnson NP, Guha A, Sdringola S. Frequent diagnostic errors in cardiac PET/CT due to misregistration of CT attenuation and emission PET images: A definitive analysis of causes, consequences, and corrections. J Nucl Med 2007;48:1112-21.

25. Gould KL, Pan T, Login C, Johnson NP, Sdringola S. Reducing radiation dose in rest-stress cardiac PET/CT by single post stress cine CT for attenuation correction: Quantitative validation. J Nucl Med 2008;49:738-45.

26. Hickey KT, Sciacca RR, Bokhara S, Rodriguez O, Chou RL, Faber TL, et al. Assessment of cardiac wall motion and ejection fraction with gated PET using N-13 ammonia. Clin Nucl Med 2004;29:243-8.

27. Moran D, Epstein Y, Keren G, Laor A, Sherez J, Shapiro Y. Calculation of mean arterial pressure during exercise as a function of heart rate. Appl Human Sci 1995;14:293-5.

28. Bailey Dl, Karp JS, Surti S. Physics and Instrumentation in PET. In: Valk PE, Bailey DL, Townsend DW, Maisey MN, editors. Positron emission tomography, basic science and clinical practice. London: Springer; 2003. p. 22. Table 2.3.

29. Cherry SR, Sorenson JA, Phelps ME. Physics in nuclear medicine. 3rd ed. Philadelphia: Saunders; 2003. p. 76. Table 6-1.

30. Well RG, de Kemp RA, Beanlands RS. Positron emission tomography instrumentation. In: Heller GV, Mann A, Hendel RC, editors. Nuclear cardiology: Technical applications. New York: McGraw-Hill Companies. Inc; 2009. p. 27. Table 2-2.

31. Christian PE, Waterstram-Rich K. PET instrumentation. In: Nuclear medicine and PET/CT: technology and techniques. 6th edn. St. Louis: Mosby; 2007. p. 315 (Table 10-1).

32. Haber SF, Derenzo SE, Uber D. Application of mathematical removal of positron blurring in positron emission tomography. IEEE Trans Nucl Sci 1990;37:1293-9.

33. Derenzo SE. Mathematical removal of positron range blurring in high resolution tomography. IEE Trans Nucl Sci 1986;33:565-9.

34. Malawi O, Podoloff DA, Kohl Myer S, Williams JJ, Stearns CW, Culp RF, et al. Performance characteristics of a newly developed PET/CT scanner using NEMA standards in 2D and 3D modes. J Nucl Med 2004;45:1734-42.

35. Mullani NA, Gould KL, Hartz RK, Hitchens RE, Wong WH, Bristow D, et al. Design and performance of POSICAM 6.5 BGO positron camera. J Nucl Med 1990;31:610-6.

36. Hutchins GD, Caraher JM, Raylman RR. A region of interest strategy for minimizing resolution distortions in quantitative myocardial PET studies. J Nucl Med 1992;33:1243-50.